LAWRENCE
LIVERMORE
NATIONAL
LABORATORY

UCRL-TR-205709

Data vs Monte Carlo Comparison of NN1 Detector

D. Lange, D. Wright, M. Burks, E. Jordan

August 4, 2004

Disclaimer

This document was prepared as an account of work sponsored by an agency of the United States Government. Neither the United States Government nor the University of California nor any of their employees, makes any warranty, express or implied, or assumes any legal liability or responsibility for the accuracy, completeness, or usefulness of any information, apparatus, product, or process disclosed, or represents that its use would not infringe privately owned rights. Reference herein to any specific commercial product, process, or service by trade name, trademark, manufacturer, or otherwise, does not necessarily constitute or imply its endorsement, recommendation, or favoring by the United States Government or the University of California. The views and opinions of authors expressed herein do not necessarily state or reflect those of the United States Government or the University of California, and shall not be used for advertising or product endorsement purposes.

Auspices Statement

This work was performed under the auspices of the U.S. Department of Energy by University of California, Lawrence Livermore National Laboratory under Contract W-7405-Eng-48.

h4doc 7v1
UCRL-TR-

Data vs. Monte Carlo Comparison of NN1 Detector

David Lange and Douglas Wright
High Energy Physics Group, N Division

Morgan Burks and Erin Jordan
Lawrence Livermore National Laboratory

July 30, 2004

Abstract

In this note, we demonstrate agreement between data and Geant4 simulations of the NN1 double-sided germanium detector using a ^{22}Na source.

1 Simulation

1.1 Detector

The heart of the NN1 detector, pictured in Figure 1, is a disk of germanium with read-out strips on each side. Only the active area is modeled; none of the cryostat or surrounding material is included. The active area of the detector is represented in the simulation by a rectangular solid 38 mm by 38 mm by 11 mm of pure germanium. The strip pitch is 2 mm in both the x and y directions, where the 38 mm by 38 mm dimensions define the xy plane (thus the z dimension is perpendicular to this plane).

1.2 Source

We mimic a ^{22}Na source with two individual lines at 511 keV and 1274 keV with the appropriate relative line strengths (in arbitrary units these correspond to 0.6429 and 0.3571, respectively). The source is placed at two meters (on the negative z axis) centered on the face of the detector. In addition we have studied the effect of moving the source to different angles with respect to the detector plane, from 0 to 90 degrees.

1.3 Physics models

We use the Geant4 [1] package for all of simulations with all default physics models. We also added the low-energy Compton-scattering package from Los Alamos[2] to include the effect of the Doppler motion of the electrons.

[1] http://geant4.web.cern.ch/geant4
[2] http://nis-www.lanl.gov/ mkippen/actsim/g4lecs

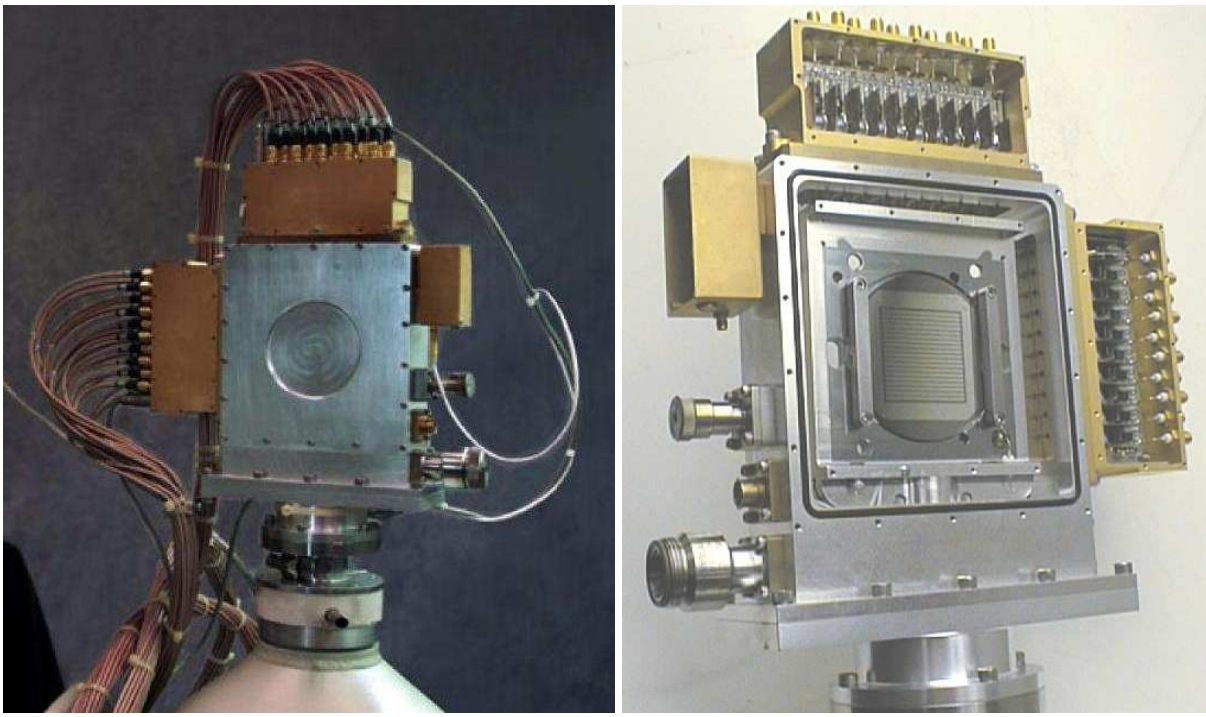

Figure 1: Photographs of NN1 detector. In the second photograph the cryostat cover is removed in order to show the germanium crystal with the read-out strips.

1.4 Event history

Geant tracks individual photons through the material until they exit the detector or interact. When the input photons interact, the location and type of interaction are recorded, and any daughter particles are tracked in the same fashion. We store the exact quantities (location, energy deposited, etc.) of the event history for all photons that enter the sensitive detector, i.e., we save a time-ordered list of Compton and photoelectric interactions for post processing.

1.5 Digitization

For each incident photon, we "digitize" the exact information and introduce detector resolution effects, so that the Monte Carlo output mimics the real data. The x and y coordinates are pixelized (converted into individual strip "hits") with a 2 mm pitch. The z coordinate is pixelized with a 0.4 mm pitch. There is no smearing of the coordinates and there is no attempt to split the deposited energy between neighboring strips, i.e., all of the deposited energy is assigned to the immediately overlying strip.

We assume an energy resolution of 2 keV at 600 keV with a square-root energy dependence. The minimum energy resolution is 1 keV. This resolution model is shown in Figure 2 and can be summarized as

$$\begin{aligned} \delta E &= 1\ \mathrm{keV}\ (E < 150\ \mathrm{keV}) \\ \delta E &= \sqrt{E/150\ \mathrm{keV}}\ (E \geq 150\ \mathrm{keV}) \end{aligned} \tag{1}$$

This energy resolution function is used to smear the energy deposited at each interaction site in the detector.

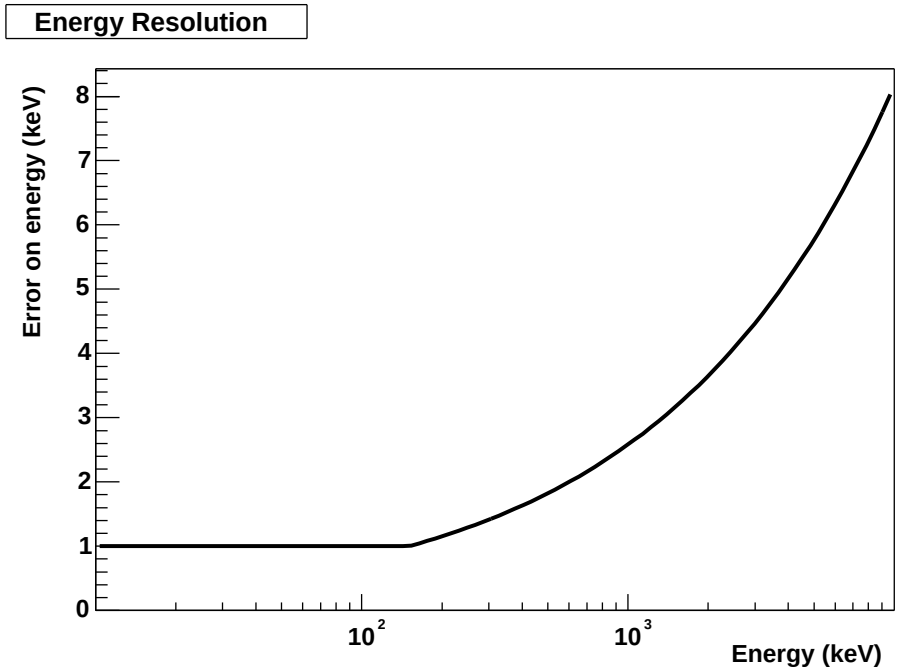

Figure 2: The detector energy resolution model used to smear the exact energies recorded by the simulation.

In the case where two or more interactions occur in the same x and/or y pixel, their energies are combined and the strip hits appear only once (as they would in data). The results of the simulation are stored in a format identical to that of the real data, so that analysis of both data and simulation are performed with the same software.

2 Results

2.1 Comparison of detector observables

A simple event selection is applied to both data and simulation. To select only photo-peak events from the 511 keV line we require that the observed energy of the event be in the range 508-514 keV. We select so-called "2-2" events where there are exactly two strip hits in the x and two hits in the y dimensions. The two hits are required to be at least three strips apart (separately for each coordinate).

Figure 3 shows the comparison between data and simulations for three quantities: the largest energy of the two measured interaction energies, the separation of the two interaction locations in the x-y plane (measured in units of the strip width), and the cosine of the Compton angle determined by the Compton formula: $\cos\theta = 1 + \frac{m_e}{E_\gamma} - \frac{m_e}{E_{\gamma'}}$. In each case, the simulation agrees well with the data.

By looking at the raw Monte Carlo information, we know that the long tail in the unphysical region below -1 in the Compton-angle distribution is due to three or more original interactions that overlap such that they appear as "2-2" events in the detector.

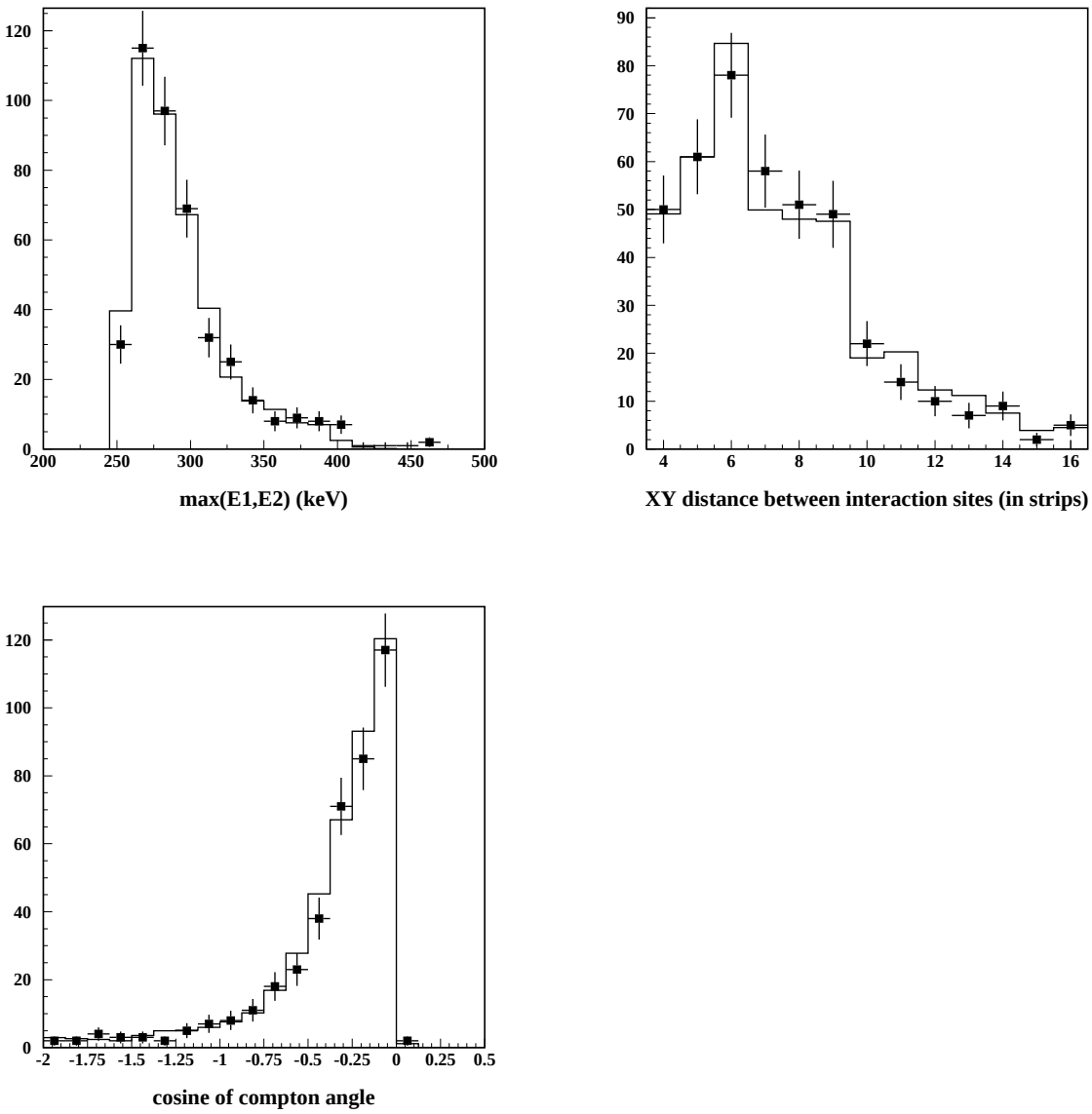

Figure 3: Comparison of data (error bars) with simulation (solid line) for the largest energy of the two measured interaction energies, the separation of the two interaction locations in the x-y plane (measured in units of the strip width), and the cosine of the Compton angle as determined by the Compton formula.

2.2 Imaging

To create a clean event sample for reconstructing images of the source, we use a more sophisticated event selection. Again we select only "2-2" events with energy around the photo-peak of the 511 keV line. We require that the two interactions be separated in both x and y by at least 2 strips (i.e., two empty strips between the hits). We require that the distance between the two interactions be greater than nine but less than 30 strips.

A single imaging algorithm, described below, was implemented and applied to both data and simulations. We assume that the highest energy interaction is the first interaction, and calculate the Compton angle. Taking the cone formed by this angle and the scattered photon direction with its apex at the first interaction location, we determine the intersection of this cone with a sphere, of radius two meters, centered at the origin of the x-y plane of the detector. Each cone produces an ellipse on the surface of the sphere. To build up the image we count the number of rings that intersect a given pixel in our field of view. Instead of spherical coordinates, we use elevation and azimuth, where the elevation is the angle above the horizon, and azimuth is the angle of the point from the sphere projected onto the horizontal plane. In our convention, the horizontal plane (horizon) corresponds to the x-z coordinates so that the y coordinate is "up."

Figure 4 shows a series of images made from data runs taken with the source directly above the detector and then moved in 15 degree increments all the way to 90 degrees. The cross-like structure in the images is a consequence of the event selection algorithm, which requires that there be a two strip separation in both strip coordinates (and thus rejecting events in which the strips are close in one dimension, but separated in the other).

For each image there is also a line-out plot of the pixel values along the elevation and azimuth coordinate axes chosen to intersect at the peak source value. The chosen axes are indicated (in black) on the image plots. Superimposed on each line-out is the corresponding plot for the data at zero degrees. Note that size and shape of the elevation plots do not change as the source location changes, but there is a dramatic effect in the azimuth plots. This is a consequence of the geometry of the detector.

When the source is normal (zero degrees) to the surface, the detector is thinnest in the nominal direction of the photon travel and thicker in the perpendicular direction. As the source moves in azimuth, the depth along the photon direction becomes thicker as that of the perpendicular correspondingly gets thinner. There also a left/right asymmetry since there is a depth asymmetry when comparing one side of the nominal photon direction to the other. The symmetry is only restored at zero and 90 degrees.

Since the error in the Compton-angle determination is minimal when the Compton angle itself is around 90 degrees[3], then lower resolution events are preferrentially rejected when the detector is thin along the initial photon direction, since it is less likely that two (or more) interactions would be contained within the detector.

The equivalent images and plots for various source locations from simulation is given in Figure 5. One can see the same general features as in the data.

In order to make a direct comparison, we superimpose the data and Monte Carlo simulation plots normalizing them by the total number of selected events. The results are shown in Figure 6. The agreement is very good for all source locations except for the case at 90 degrees. This is perhaps not a surprise since there was no attempt in the Monte Carlo to implement the cryostat walls or even the non-instrumented portion of the germanium crystal.

[3]See UCRL-TR-202187 (h4_doc6) for analytic calculations of the Compton-angle error.

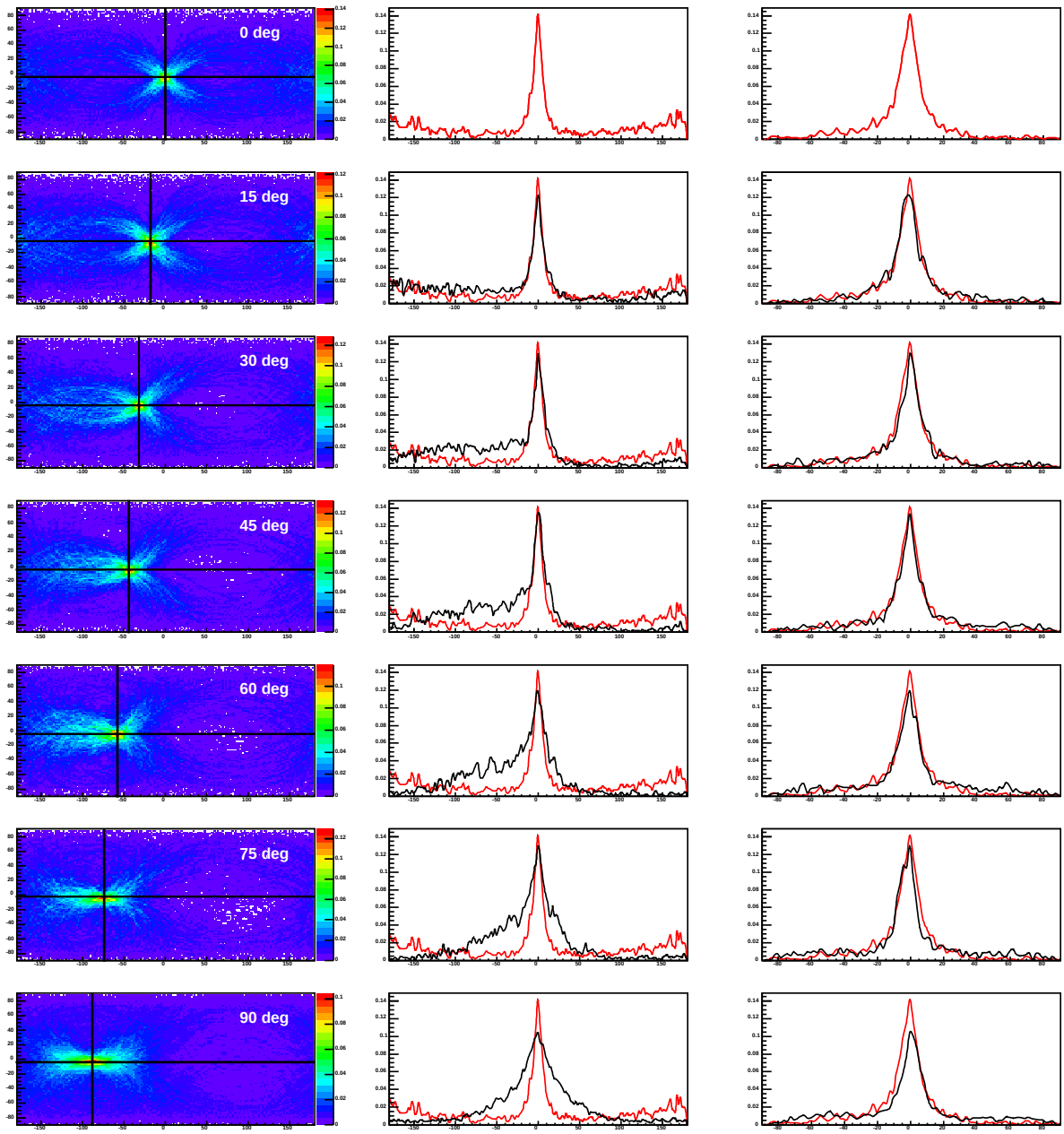

Figure 4: Data images for various source locations. For each image there are plots of the pixel values along the elevation and azimuth coordinate axes (shown in black on the image) chosen to intersect at the peak source value.

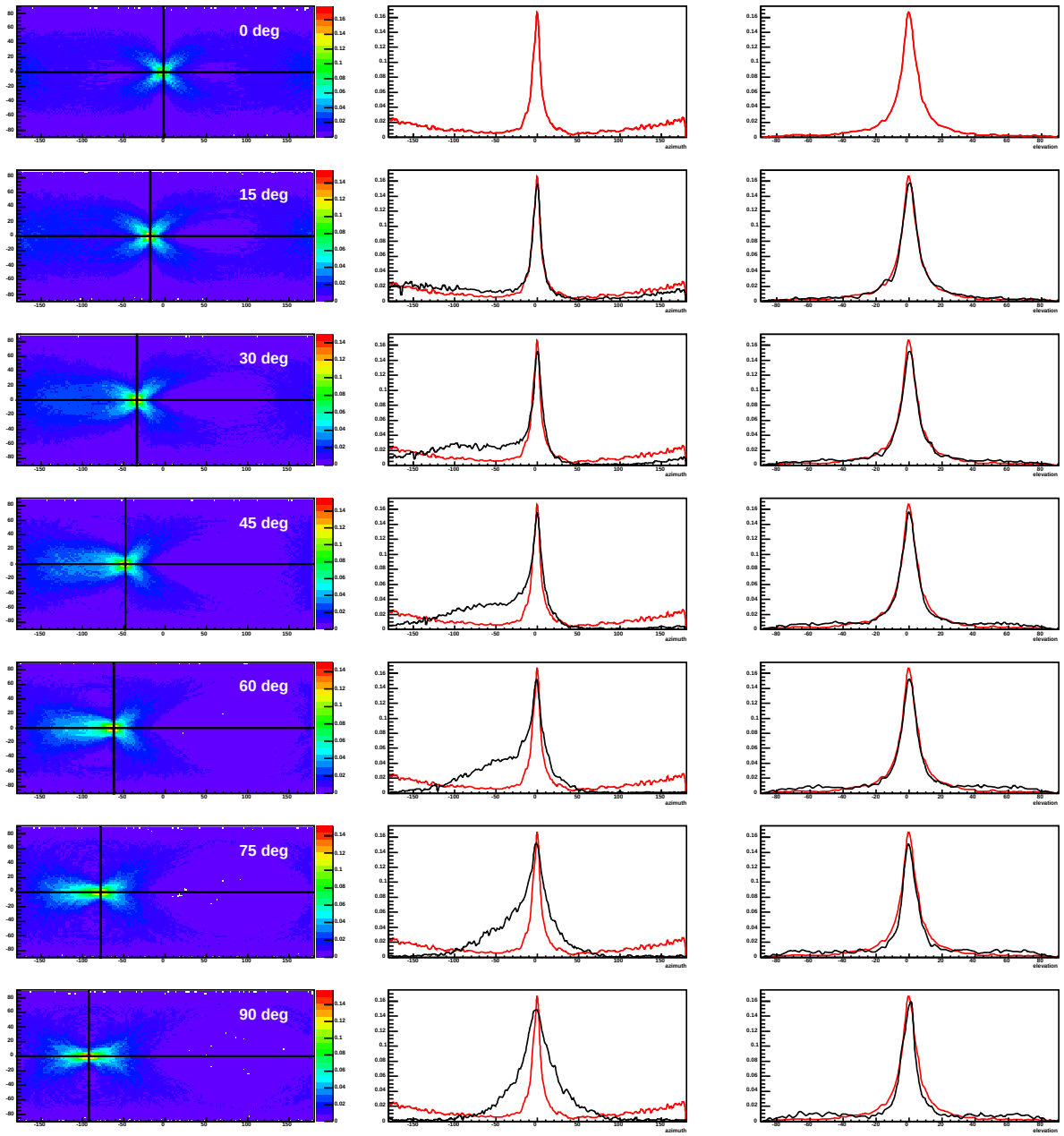

Figure 5: Simulation images for various source locations. For each image there are plots of the pixel values along the elevation and azimuth coordinate axes (shown in black on the image) chosen to intersect at the peak source value.

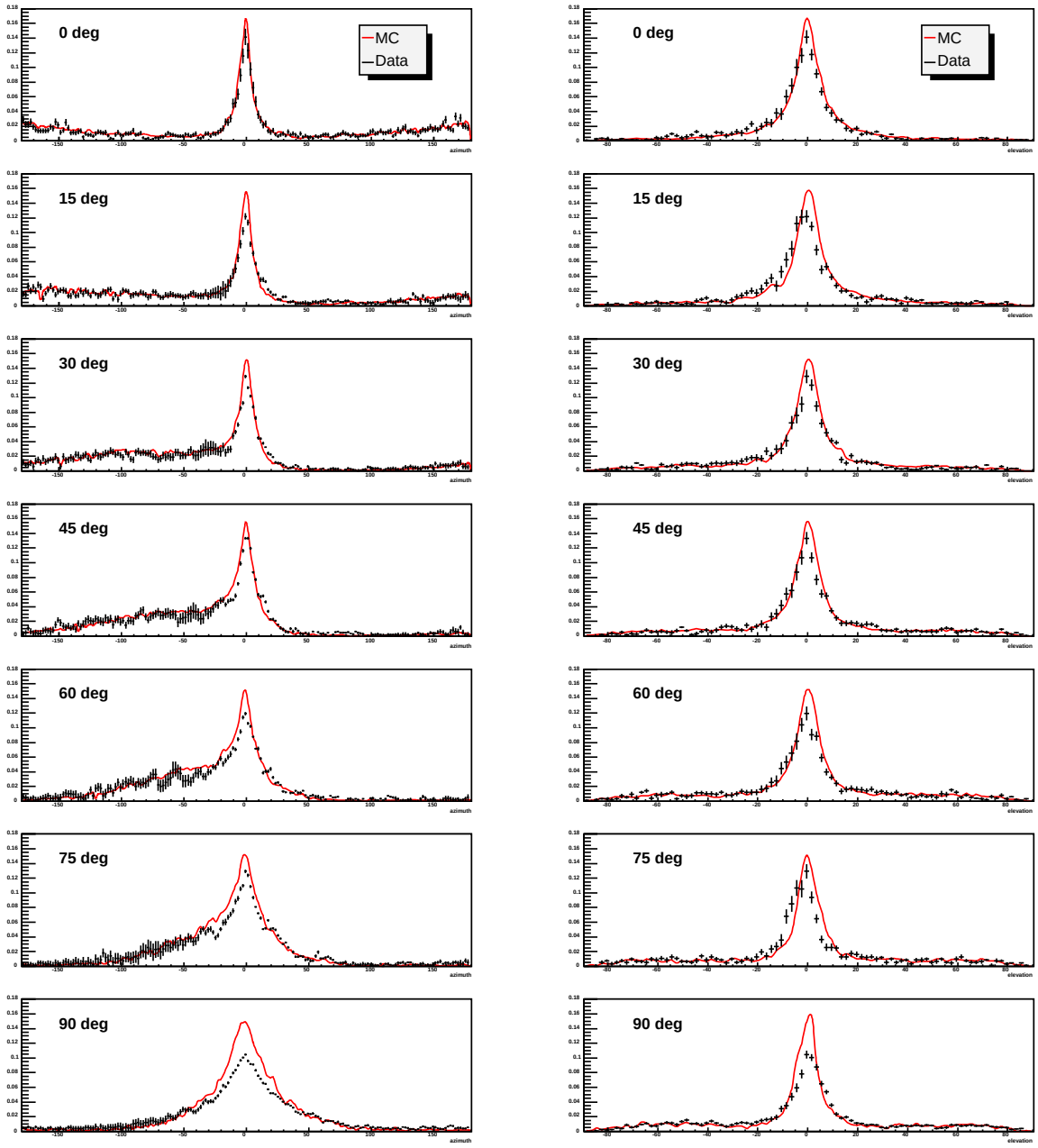

Figure 6: Data (error bars) and simulation (red line) distributions in azimuth and elevation through the peak source value, normalized by the number of selected events.